Computational Studies of Transition Metal Selectivity of Octapeptide Repeat Region of Prion Protein (PrP)

Krishna K. Pandey,*,‡ James P. Snyder,† Dennis C. Liotta,† and Djamaladdin G. Musaev*,†

Cherry L. Emerson Center for Scientific Computation and Department of Chemistry, Emory University, Atlanta, Georgia 30322, and School of Chemical Sciences, Devi Ahilya University Indore, Indore 452001, India

Received: October 16, 2009; Revised Manuscript Received: November 12, 2009

We have presented a detailed theoretical (density functional theory and ONIOM) study on the structure and M−PrP (prion protein) interaction on various prion models, M(PrP) systems (where PrP = HGG, HGGGW·$3H_2O$, and PrP(61−84), and M = Zn, Cu, Ni, Co, Fe, Mn). It was shown that the geometry of the complex [Mn(HGGGW)(H_2O)]·$2H_2O$ is quite different for M = Mn(III) and Mn(II), and partial unfolding occurs only for the M = Mn(III). In [Zn{PrP(61−84)}], Zn(II) forms a bond with carbonyl oxygen of the Pro(84) residue in the axial position. The coordination of transition metal ions to PrP(61−84) induces the significant geometrical changes in the PrP(61−68) and Prp(69−76) octapeptide repeat regions. The Trp(65) and Trp(73) residues come closer to each other. The glutamines Gln(67) and Gln(75) also come closer to one another and result in the formation of a hydrogen bond between the carbonyl carbon of Gln(67) and one of the NH_2 hydrogens of Gln(75). A specific aggregatory effect is found for Co(II) and Mn(II). The relative binding ability of the metal ions increases in the order Zn(II) < Mn(II) < Cu(II) < Fe(II) < Co(II) < Ni(II). The PrP is most distorted upon binding to Co(II) and least distorted upon binding to Zn(II).

Introduction

Prion diseases, or transmissible spongiform encephalopathies, are fetal neurodegenerative disorders that affect the central nervous system of both humans and animals. Human forms of prion diseases include Creutzfeld−Jacob disease, Gerstamnn−Straussler−Scheinker disorders, fetal familial insomnia, and kuru. Animal forms include scrapie in sheep and goat, chronic wasting disorder in mule, deer, and elk, and bovine spongiform encephalophy in cattle.[1−3] Some prion protein (PrP)-associated diseases involve an infectious agent hypothesized to be an altered confirmation of PrP known as PrP^{Sc}. Conversion of PrP to PrP^{Sc} is a central event in the etiology of transmissible PrP associated diseases, the mechanism of which remains poorly understood. It is believed that inside the cell, PrP and PrP^{Sc} exist in equilibrium with the latter below detectable limits. Exposure to divalent, trace element, metal dications may induce structural changes that affect the equilibrium between PrP and PrP^{Sc} and increase the PrP^{Sc} levels.[4] Therefore, it is imperative to investigate the interactions of metals with cellular prion proteins. A detailed understanding of the role of metals in the deformation of PrP and the relative binding strengths of relevant metals may ultimately enable development of a successful treatment strategy for neurodegenerative conditions. As a result, the interaction of metals with cellular prion proteins has been the subject of numerous experimental and theoretical studies.

Both experimental[5−16] and molecular dynamics studies[14,17,18] have suggested a number of binding sites for metal dications in PrP (60−231). One such site is the octarepeat region of [M(PHGGGWGQ)] (see Scheme 1), which can selectively bind four metal ions. Another metal binding site is [M(GGGTH)] in the PrP(92−96) sequence.[12−15]

SCHEME 1: Metal Binding Sites in Prion Protein (PrP)[a]

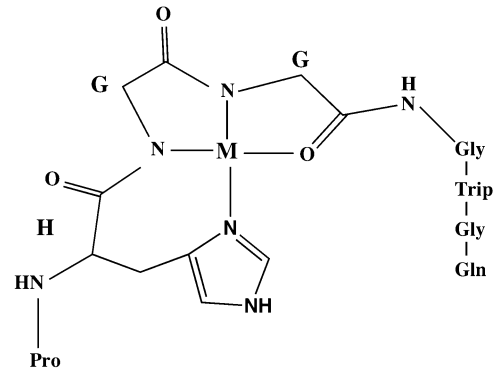

[M(PHGGGWGQ)]

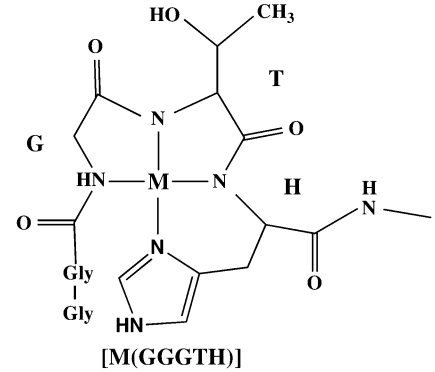

[M(GGGTH)]

[a] [M(PHGGGWGQ)] is one of the four octarepeat regions, and [M(GGGTH)] PrP(92−96) is the fifth binding site.

Coordination to a C-terminal fragment has also been reported.[16−18] In total, from four to seven copper atoms have been suggested to bind purified PrP preparations from mouse and human brain, respectively.[19,20] Despite the wide recognition

* Corresponding authors. E-mails: (D.G.M.) dmusaev@emory.edu; (K.K.P.) kkpandey.schem@dauniv.ac.in.
‡ Devi Ahilya University Indore.
† Emory University.

10.1021/jp909945e
Published on Web 12/18/2009

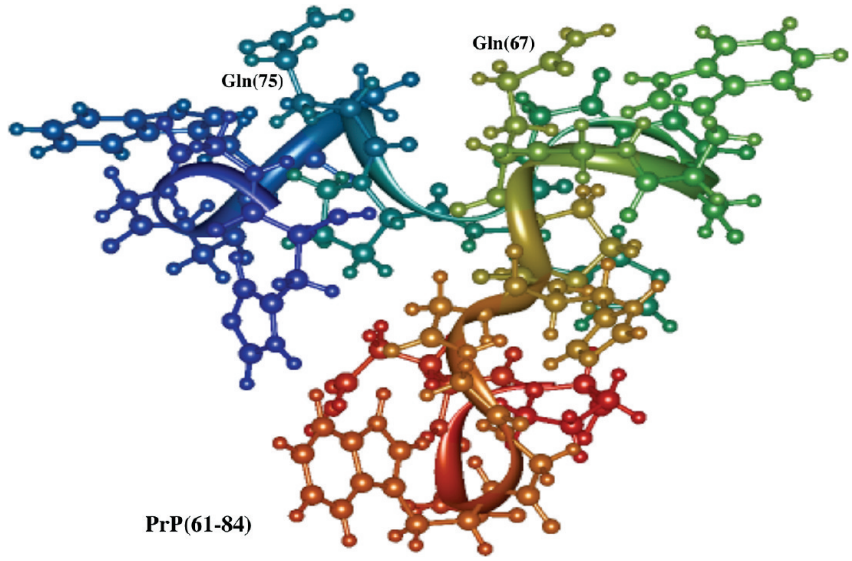

Figure 1. The structures of the PrP(61−84) (see ref 39).

of PrP as a copper-binding protein, interaction with other divalent metal cations (Zn(II), Ni(II), Mn(II)) has also been reported,[21−26] but this is a subject of intense controversy. Brown et al.[21] found that only Mn^{2+} and Ni^{2+} could substitute for Cu^{2+}. In contrast, Harris et. al[27] and Garnett and Viles[28] have reported that Mn^{2+} does not bind to the octapeptide repeat region of PrP. In addition, Giese and co-workers have reported that Mn(II) displays a specific, strong, proaggregatory effect at low millimolar concentration to a greater extent than Cu(II), Ni(II), Co(II), or Zn(II). Moreover, the phenomenon could be blocked by Cu(II) at nanomolar concentration. Co(II) also displays a significant proaggregatory effect that, in contrast to the effect of manganese, could not be blocked by Cu(II).[29] Thus, these studies indicate that Co(II) binds more strongly than Mn(II). Cu(II) has recently been shown to inhibit the conversion of recombinant PrP(23−230) to amyloid fibrils at micromolar concentration and at pH 7.2.[30] Thus, the role of metal cations and their coordination to PrP is evidently rather complex, and even the fact that the prion protein is directly involved in copper homeostasis is still a matter of debate.

In this context, detailed quantum mechanical studies of these issues could prove extremely useful. Previously, the binding of copper to PrP models has been theoretically investigated.[14,17,18,31,32] However, to provide a complete picture of metal binding to the octapeptide repeat domains of the protein and provide novel insight that can not be obtained experimentally, we report here a detailed theoretical investigation of the transition metal binding through the PHGGGWGQ sequence in [M(HGG)], [M(HGGGW)(H_2O)]·$2H_2O$, and [M{PrP(61−84)}] [PHGGG-WGQ-PHGGGWGQ-PHGGGWQ-M(II)] (where M = Zn(II), Cu(II), Ni(II), Co(II), Fe(II), Mn(II)). We also study the Mn(III) binding in complexes $[Mn(HGG)]^+$ and [Mn(HGGGW)-(H_2O)]·$2H_2O$. We believe this systematic approach will permit answers to the following questions: (a) Does Cu(II) possess a higher affinity for PrP than dications of other first-row transition metals? (b) Does Mn(II) bind to the octarepeat region of the PrP? (c) Does Mn(III), obtained by oxidizing Mn(II), bind strongly to PrP? Which metal dication deforms PrP to the greatest extent?

Computational Details

The quantum mechanical calculations described here have been performed at the nonlocal DFT[33,34] and ONIOM[35] levels

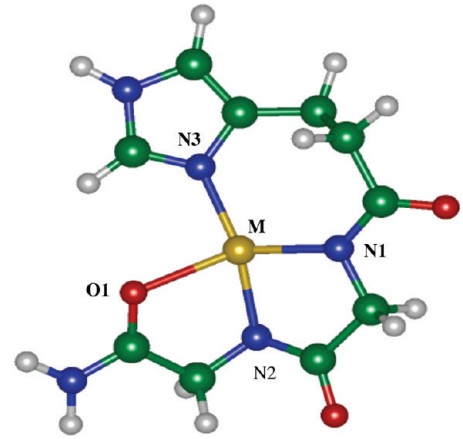

Figure 2. Optimized structure of the [M(HGG)] model systems and the notations of the important atoms. The calculated important geometry parameters of these systems are given in Table 1 (their full geometries are provided in the Supporting Information).

of theory. DFT calculations for the [M(HGG)] (model I) and [M(HGGGW)(H_2O)]·$2H_2O$ (model II) complexes were performed using the exchange functional of Becke[36] and the correlation functional of Perdew[37] (BP86). In these calculations, the TZVP standard basis sets of Ahlrichs and co-workers have been used.[38] Coordinates of PrP(61−84) were taken from the pdb file 1OEI.pdb[39] (see Figure 1), and transition metal dications were added to the PHGGGWGQ sequence in [M(HGG)], [M(HGGGW)(H_2O)]·$2H_2O$, and [M{PrP(61−84)}], as shown in Scheme 1. Geometries of the reported structures have been optimized without symmetry constraints. Solvent effects were evaluated by performing single-point energy calculations at the PCM continuum model simulating water as solvent ($\varepsilon = 78.39$) using the gas-phase optimized geometries. The electronic structures of the complexes were examined by NBO analysis.[40]

In the context of the ONIOM (QM:MM)[40] approach, the [M{PrP(61−84)] prion fragment was divided into two subsystems (layers), each of which is described at a different level of theory. Subsystem 1 (or "model" system) was chosen to be model I, [M(HGG)], which is described at the highest theoretical level used in this paper; namely, the BP86/TZVP level. Subsystem 2 (or lower layer) was selected to represent the remainder of the [M{PrP(61−84)] fragment, whichis treated

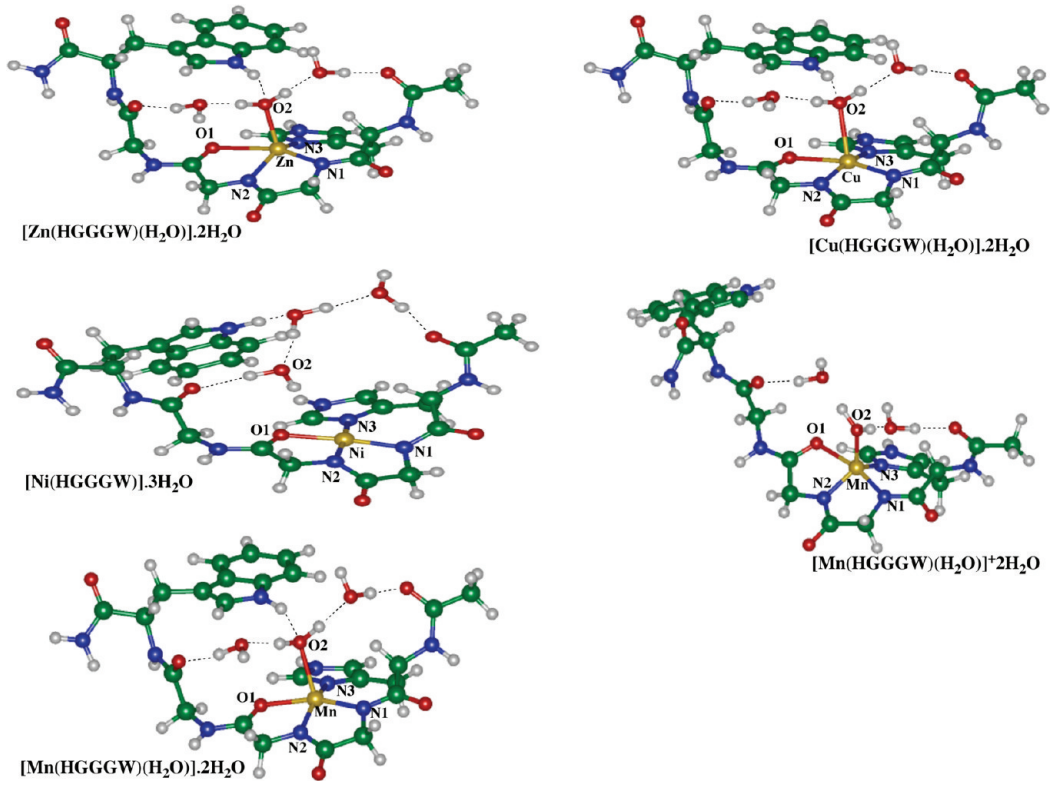

Figure 3. Optimized structures of the $[Mn(HGGGW)(H_2O)]^+ \cdot 2H_2O$, $[Mn(HGGGW)(H_2O)] \cdot 2H_2O$, and $[Ni(HGGGW)] \cdot 3H_2O$ systems, and the notations of the important atoms. The calculated important geometry parameters of these systems are given in Table 1 (their full geometries are provided in the Supporting Information).

with the AMBER force field. In these calculations, Babu and Lim's force field parameters for transition metals were used.[41]

All calculations were carried out with the Gaussian03 program.[42] MO pictures were made by using the MOLDEN program.[43]

Binding interactions in the [M(HGG)] (M = Zn(II), Cu(II), Ni(II), Co(II), Mn(II)) complexes between metal M^{2+} and HGG^{2-} fragments have been analyzed without symmetry restrictions. Deformation energies (defined as an energy induced by deformation of geometries of HGG^{2-} upon coordination to the transition metal centers), E(DEF), of HGG^{2-} prion fragments were estimated by application of the following equation:

$$E(\mathrm{DEF}) = E(\mathrm{HGG}^{2-})_{(\text{in complex})} - E(\mathrm{HGG}^{2-})_{(\text{equilibrium geometry})} \quad (1)$$

Results and Discussion

A. Geometries of the [M(HGG)] and [M(HGGGW)-(H$_2$O)]·2H$_2$O Complexes. To elucidate the spin state and metal-induced geometry changes of the PrP^{2-} ligand, we studied 12 model complexes of the octapeptide repeat region [M(HGG)] and $[M(HGGGW)(H_2O)] \cdot 2H_2O$ (M = Zn(II), Cu(II), Ni(II), Co(II), Fe(II), Mn(II)) in the gas phase. Optimized structures of the [M(HGG)] and $[M(HGGGW)(H_2O)] \cdot 2H_2O$ complexes for several lower-lying electronic states are depicted in Figures 2 and 3, respectively; their important geometry parameters are presented in Table 1.

As seen from the data in Table 1, all complexes studied exhibit nearly square planar geometries around the metal center, with the exception of [Zn(HGG)], which is distorted toward tetrahedral geometry with angles of ∠N2−Zn−N3 = 152.6° and ∠N1−Zn−O1 = 143.3°. The covalent bonds M−N1 and M−N2 are somewhat shorter than the donor bonds M−N3 and M−O1. In general, the M−O bond is found to be longer than the M−N bonds.

The geometries of all $[M(HGGGW)(H_2O)] \cdot 2H_2O$ complexes, except those for M = Zn and Ni, are found to be approximately square pyramidal around the M center with four of the M(II) coordination sites occupied by the HGG fragment of the $(HGGGW)(H_2O)] \cdot 2H_2O$ unit. One of the water molecules is coordinated in an axial position, and the other two water molecules are H-bonded to the coordinated water and other amino acids of (HGGGW). The M ions interact with the Trp residue through hydrogen bonding between the oxygen of a coordinated water and hydrogen of the indole NH. The water in the fifth coordination site is weakly bonded to Cu(II) (Cu−O2 = 2.477 Å) and Fe(II) (Fe−O2 = 2.591 Å). The observed metal−O2 bond distances are Zn(II)−O2, 2.108 Å; Co(II)−O2, 2.290 Å; Mn(II)−O2, 2.225 Å, and Mn(III)−O2, 1.844 Å. The structure of the $[M(HGGGW)(H_2O)] \cdot 2H_2O$ (M = Cu(II), Co(II), Fe(II), Mn(II)) complexes closely resembles the crystal structure of Cu(II)−HGGGW.[44] The structure of $[Ni(HGGGW)] \cdot 3H_2O$ is nearly square planar around the Ni(II) center: The coordinated water has moved toward Trp and forms a strong hydrogen bond (O2−HN = 1.824 Å) with the NH group of indole. The calculated Ni(II)−O2 distance, 3.821 Å, indicates no interaction between the Ni center and water molecule. This structural difference between the $[Ni(HGGGW)] \cdot 3H_2O$ and other presented systems could be explained by the preference of the Ni(II) dication for formation of a square planar structure. The coordination geometry around the Zn center of [Zn(HGGGW)-(H$_2$O)]2H$_2$O is nearly trigonal−bipyramidal with O2, N2, and N3 atoms lying in an equatorial plane. The calculated ∠N2−Zn−N3 and ∠O2−Zn−O1 angles are 136.2° and 83.2°, respectively.

TABLE 1: Selected Optimized Geometrical Parameters[a] for [M(HGG)] (first line), Human [M{PrP(61−84)}] (second line) and [M(HGGGW)(H_2O)]2H_2O Complexes (third line)

	M−N1	M−N2	M−N3	M−O1	⟨N1−M−N2	⟨N2−M−N3	⟨N3−M−O1	⟨N1−M−N3	⟨N1−M−O1	⟨N2−M−O1
Zn(II, 1)	1.987	1.966	1.976	2.240	86.1	152.6	94.2	113.3	143.3	79.6
	[1.962]	[1.909]	[1.974]	[2.774]	[90.5]	[152.9]	[84.5]	[114.4]	[158.5]	[73.6]
	(2.036)	(1.991)	(2.043)	(2.476)	(83.6)	(136.2)	(88.8)	(107.0)	(157.1)	(73.5)
Cu(II, 2)	2.006	1.916	1.973	2.137	83.7	169.2	89.7	107.0	163.3	79.6
	[1.988]	[1.906]	[1.984]	[2.197]	[84.6]	[159.9]	[93.5]	[108.3]	[150.1]	[80.9]
	(2.009)	(1.938)	(2.009)	(2.173)	(82.3)	(159.6)	(92.2)	(104.3)	(160.7)	(78.9)
Ni(II, 1)	1.881	1.843	1.931	1.934	83.9	171.0	91.9	100.3	167.7	84.1
	[1.901]	[1.840]	[1.970]	[1.973]	[83.6]	[164.2]	[91.9]	[102.7]	[165.2]	[82.8]
	(1.888)	(1.842)	(1.936)	(1.936)	((83.7)	(171.5)	(91.4)	(101.3)	(167.3)	(83.8)
Ni(II, 3)	1.933	1.945	1.989	2.122	84.2	162.4	92.1	110.1	146.7	79.9
	[1.948]	[1.917]	[1.963]	2.351]	[86.1]	[166.3]	[92.7]	[106.8]	[149.2]	[77.7]
	(1.938)	(1.941)	(1.987)	(2.136)	(84.2)	(163.5)	(91.4)	(109.9)	(148.6)	(79.5)
Co(II, 2)	1.895	1.859	1.931	1.949	84.9	172.3	89.3	102.5	168.2	83.4
	[1.907]	[1.820]	[1.977]	[1.991]	[84.3]	[165.9]	[96.4]	[97.5]	[165.3]	[83.4]
	(1.938)	(1.879)	(1.988)	(2.019)	(83.0)	(162.9)	(92.1)	(101.0)	(163.7)	(81.6)
Co(II, 4)	1.961	1.929	2.009	2.141	84.6	151.9	96.7	110.0	147.3	80.0
	(2.007)	(1.963)	(2.042)	(2.439)	(83.6)	(133.3)	(87.4)	(106.0)	(157.4)	(74.1)
Fe(II, 1)	1.850	1.897	1.956	1.930	84.5	172.7	90.9	102.8	149.7	83.0
	[1.875]	[1.836]	[2.051]	[2.199]	83.8]	[171.6]	[96.7]	[99.3]	[163.1]	[81.2]
	(1.959)	(1.869)	(1.995)	(2.047)	(82.7)	(155.4)	(91.2)	(103.4)	(163.0)	(80.4)
Fe(II, 3)	1.932	1.863	1.985	1.987	84.5	170.8	89.0	104.1	166.8	82.4
	[1.889]	[1.848]	[2.015]	[2.045]	[84.6]	[167.5]	[96.9]	[100.1]	[158.7]	[81.5]
	(1.940)	(1.881)	(2.024)	(2.036)	(83.2)	(161.8)	(90.6)	(102.8)	(163.7)	(81.3)
Fe(II, 5)	1.998	1.992	2.042	2.200	82.8	157.5	91.2	113.2	154.1	76.6
	(2.063)	(2.006)	(2.096)	(2.382)	(74.6)	(131.3)	(88.6)	(104.1)	(155.2)	(74.6)
Mn(II, 2)	1.951	1.891	2.026	2.020	83.6	167.8	90.5	105.3	163.9	81.3
	[1.912]	[1.905]	[2.048]	[2.063]	[83.9]	[168.6]	[97.3]	[101.3]	[152.0]	[81.7]
	(1.978)	(1.916)	(2.065)	(2.100)	(82.5)	(154.4)	(90.5)	(102.8)	(161.3)	(79.9)
Mn(II, 4)	1.964	1.915	2.029	2.005	83.4	169.8	89.9	106.2	163.8	80.5
	(1.990)	(1.927)	(2.070)	(2.098)	(82.2)	(158.1)	(91.9)	(102.3)	(161.3)	(80.1)
Mn(II, 6)	2.053	2.048	2.093	2.219	81.5	150.9	101.5	112.9	141.3	76.4
	(2.117)	(2.079)	(2.153)	(2.354)	(79.1)	(136.2)	(92.8)	(103.8)	(152.2)	(73.6)
Mn(III, 1)	1.827	1.812	1.974	1.950	85.3	145.2	96.3	105.8	154.2	84.0
	(1.933)	(1.816)	(1.952)	(2.118)	(85.9)	(122.1)	(88.2)	(101.4)	(166.0)	(80.4)
Mn(III, 3)	1.910	1.873	2.007	1.972	83.5	162.5	91.7	105.0	163.1	81.2
	(1.932)	(1.862)	(2.042)	(2.050)	(84.0)	(143.4)	(88.6)	(102.4)	(164.6)	(80.7)
Mn(III, 5)	1.924	1.897	2.027	1.976	83.2	166.2	90.1	106.7	163.2	80.6
	(1.952)	(1.919)	(2.063)	(2.020)	(82.2)	(152.4)	(91.4)	(101.9)	(161.0)	(79.8)

[a] Distances, Å; angles, degree.

It has been reported that cellular enzymes tend to oxidize Mn(II) to Mn(III).[45,46] Therefore, model complexes of Mn(III), $[Mn(HGG)]^+$, and $[Mn(HGGGW)(H_2O)]^+ \cdot 2H_2O$ have also been optimized at their singlet, triplet, and quintet spin states. As expected, Mn(III) is more strongly bound with PrP^{2-} models than Mn(II). The geometry about Mn(III) in $[Mn(HGG)]^+$ is nearly tetrahedral, with bond angles ∠N2−Mn−N3 = 145.2° and ∠N1−Mn−O1 = 154.2°. The geometry of the complex $[Mn(HGGGW)(H_2O)]^+ \cdot 2H_2O$ for Mn(III) is quite different from the geometries of the analogous M(II) complex. As seen in Figure 3, the Trp residue moves away (unfolding) in the Mn(III) complex, and there is no hydrogen bond between the coordinated water oxygen and the indole NH hydrogen. This distance is calculated to be 9.042 Å in the Mn(III) complex, whereas it is a 2.026 Å in the Mn(II) complex. The geometry around the Mn(III) center is trigonal−bipyramidal with N2, N3, and O2 atoms in the equatorial plane. The partial unfolding of the globular domain may allow for recognition between the PrP(90−120) regions, thereby facilitating formation of PrP^{Sc}.

B. Geometries of [M{PrP(61−84)}]. To account for protein environment effects on the calculated geometries and energies, we have studied eight complexes of [M{PrP(61−84)}] (M = Zn (II, 1), Cu(II, 2), Ni(II, 1), Ni(II, 3), Co(II, 2), Fe(II, 1), Fe(II, 3), Mn(II, 2)) using the ONIOM (BP86:AMBER) approach. In these calculations, [M{PrP(61−84)}] is divided into two parts: (i) model [M(HGG)] and (ii) the remainder of the system. Atoms of the model [M(HGG)] are described at the DFT/BP86 level; other atoms are treated at the AMBER level. In Figures 4 and 5, we show the optimized structures of three specific cases: the complexes for M = Zn, Cu, and Co. In Figure 5, we present uncoordinated PrP−ligand.

The important geometric parameters of all modeled [M{PrP(61−84)}] systems are presented in Table 1 (in the third line), and full geometries of these complexes given in the Supporting Information. As seen from Figure 3 and Table 1, inclusion of the protein environment into the calculations significantly changes the geometries of the model systems. For example, in [Zn{PrP(61−84)}], Zn(II) forms a bond with the carbonyl oxygen of the Pro(84) residue in the axial position, which could not be observed for model-only studies. Thus, the structure of [Zn{PrP(61−84)}] proved to be nearly square pyramidal around the Zn(II) center with a shorter Zn−O(CO) bond distance, 2.37 Å, and a longer Zn−O1 bond distance, 2.77 Å. In the [Cu{PrP(61−84)}] complex, Cu−N1 and Cu−N2 bonds become shorter and Cu−N3 and Cu−O1 distances become longer than in [Cu(HGG)]. Furthermore, the geometry around the Cu(II) center tends slightly toward tetrahedral. That is, the calculated N2−Cu−N3 and N1−Cu−O1 bond angles decrease from 169.2° and 163.3° in model system [Cu(HGG)] to 159.9° and 150.1° in [Cu{PrP(61−84)}], respectively. In addition, the M−N1, M−N3, and M−O1 bond distances are elongated in complexes [M{PrP(61−84)}] (M = Ni(II, 1), Co(II, 2), Fe(II, 3), and Mn(II, 2)) as compared to the model system [M(HGG)].

Important geometrical changes occurring in the PrP(61−68) and Prp(69−76) octapeptide repeats resulting from coordination of M(II) cations to the PrP(77−84) octarepeat region of PrP(61−84) are presented in Table 2.

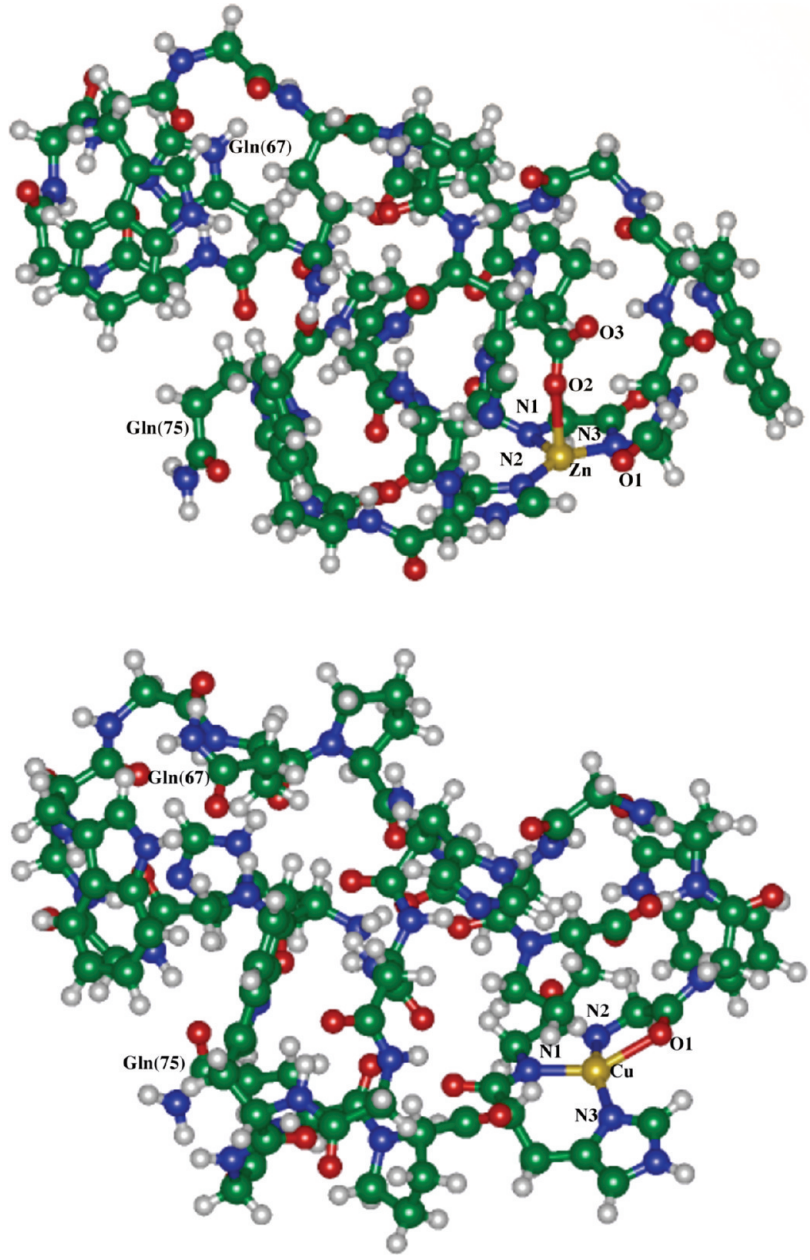

Figure 4. Optimized structures of the [M{PrP(61−84)}] (M = Zn, Cu) and the notations of the important atoms. The calculated important geometry parameters of these systems are given in Table 1 (their full geometries are provided in the Supporting Information).

As seen in Figure 5 and Table 2 for [Co{PrP(61−84)}], the Trp(65) and Trp(73) and the Gln(67) and Gln(75) residues move toward each other, respectively. It is important to note that in all the studied systems, the Trp(65) and Trp(73) residues come close to each other. In free PrP(61−84), the HN···NH distance between NH groups of Trp(65) and Trp(73) is 14.47 Å, which reduces to the range 11.26−5.68 Å (Table 2). The larger reduction of the HN···NH distance is found in [Cu{PrP(61−84)}] (5.68 Å), whereas a smaller reductive effect has been observed in [Fe{PrP(61−84)}] (11.26 Å).

It is worth noting that within the octapeptide repeat region, Gln(75) is the only side chain bearing a functional group that does not participate in metal binding. In [Cu{PrP(61−84)}], coordination of Cu(II) to the octarepeat region of PrP(61−84) does not change the geometric configuration of the octarepeat domain. This finding is in good agreement with the experimental observations.[44] Remarkably, these calculations reveal a noticeable aggregatory effect only for Co(II) and Mn(II) complexes. Indeed, as seen in Figure 5, glutamines Gln(67) and Gln(75) of the optimized [Co{PrP(61−84)}] complex (and that of [Mn{PrP(61−84)}], as well; not shown) are suggested to approach one another intramolecularly. Thus, group separations in the Co(II) complex are $H_2N\cdots NH_2$, 4.84 Å; O(CO)···O(CO), 4.80 Å; $H_2N\cdots$O(CO), 2.84 Å, whereas the Mn(II) complex reveals identical values ($H_2N\cdots NH_2$, 4.84 Å; O(CO)···O(CO), 4.80 Å; $H_2N\cdots$O(CO), 2.84 Å). The latter values can be compared to free PrP(61−84) in which the same separations are 2−3 times longer: $H_2N\cdots NH_2$, 8.29 Å; O(CO)···O(CO), 10.81 Å; $H_2N\cdots$O(CO), 10.27 Å. The formation of a hydrogen bond between the carbonyl carbon of Gln(67) and one of the Gln(75) NH_2 hydrogens results. The calculated O···HN separations are 1.85 and 1.85 Å in the Co(II, 2) and Mn(II, 2) complexes, respectively, as compared to an O−HN distance of 9.60 Å in free PrP(61−84). Thus, we observe that metalated [Co{PrP(61−84)}] and [Mn{PrP(61−84)}] complexes bring together distal glutamine centers in two octarepeat domains of the free peptide.

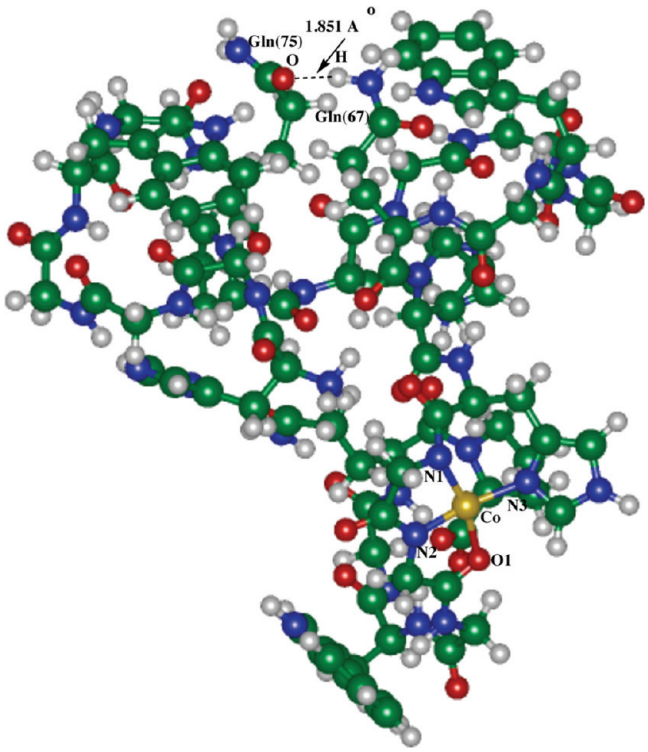

Figure 5. Optimized structures of the [Co{PrP(61−84)}]. The calculated important geometry parameters of this system are given in Table 1 (their full geometries are provided in the Supporting Information).

TABLE 2: Important Geometrical Changes[a] in the First and Second Octarepeat Regions, PrP(61−68) and PrP(69−76), Respectively, upon Coordination of M(II) Cations to the Third Octarepeat Region, PrP(77−84), of PrP(61−84)

	[Trp(65)]−[Trp(73)]	[Gln(67)−Gln(75)]			
	HN−NH	H_2N−NH_2	O(CO)−O(CO)	H_2N−O(CO)	O(CO)−HNH
PrP(61−84)	14.47	8.29	10.81	10.17	9.60
[Zn{PrP(61−84)}]	7.24	11.49	8.35	10.08	10.61
[Cu{PrP(61−84)}]	5.68	11.86	8.45	10.34	10.02
[Ni{PrP(61−84)}]	7.54	8.51	7.11	6.65	6.23
[Co{PrP(61−84)}]	7.16	4.84	4.80	2.84	1.85
[Fe{PrP(61−84)}]	11.26	10.57	9.80	11.53	2.03
[Mn{PrP(61−84)}]	7.17	4.84	4.80	2.84	1.85

[a] Distances, Å.

This may be of significance, as Millhauser and co-workers[44] have suggested that such glutamine cross-linked PrP proteins may act as molecular signal stimulating endocytosis.

Bonding Analysis in [M(HGG)], [M(HGGGW)(H_2O)]·$2H_2O$ and [M{PrP(61−84)}]. Below, we analyze the nature of M−octarepeats bonding in the title systems. In the analysis, we use the conventional indices, which are frequently used to characterize the bonding in molecules; namely, bond orders and atomic charges. The Wiberg bond indices[47] and the natural bond orbital (NBO)[43] charge distributions of the [M(HGG)] (first line) and [M(HGGGW)(H_2O)]·$2H_2O$ (second line) complexes are presented in Tables 3 and 4.

As seen from the tables, Wiberg bond indices for the M−N1, M−N2, M−N3, and M−O1 bonds of all studied complexes are very small, indicating that these bonds have a substantial degree of ionic character. Furthermore, the results reveal that M−N1 and M−N2 bonds are stronger than M−N3 and M−O1 bonds. The calculated NBO charge distribution indicates that the metal atoms of these complexes always carry a positive charge, whereas their N1, N2, N3, and O1 atoms, as well as

TABLE 3: Wiberg Bond Indices in [M(HGG)] and [M(HGGGW)(H_2O)]·$2H_2O$[a] Models

	M−N1	M−N2	M−N3	M−O1	M−O2
Zn(II, 1)	0.21	0.22	0.19	0.07	
	(0.16)	(0.19)	(0.15)	(0.04)	(0.09)
Cu(II, 2)	0.23	0.25	0.20	0.09	
	(0.22)	(0.23)	(0.18)	(0.08)	(0.04)
Ni(II, 1)	0.48	0.44	0.29	0.22	
	(0.46)	(0.45)	(0.29)	(0.22)	(0.00)
Ni(II, 3)	0.36	0.26	0.21	0.11	
	(0.34)	(0.26)	(0.21)	(0.10)	(0.02)
Co(II, 2)	0.47	0.45	0.31	0.24	
	(0.45)	(0.45)	(0.29)	(0.20)	(0.08)
Co(II, 4)	0.33	0.32	0.21	0.11	
	(0.25)	(0.28)	(0.19)	(0.05)	(0.13)
Fe(II, 1)	0.44	0.79	0.35	0.27	
	(0.50)	(0.58)	(0.37)	(0.24)	(0.33)
Fe(II, 3)	0.53	0.52	0.31	0.24	
	(0.49)	(0.50)	(0.29)	(0.21)	(0.05)
Fe(II, 5)	0.32	0.30	0.22	0.11	
	(0.24)	(0.27)	(0.18)	(0.06)	(0.14)
Mn(II, 2)	0.54	0.55	0.31	0.25	
	(0.49)	(0.51)	(0.30)	(0.20)	(0.14)
Mn(II, 4)	0.51	0.50	0.30	0.24	
	(0.46)	(0.47)	(0.27)	(0.19)	(0.02)
Mn(II, 6)	0.28	0.27	0.20	0.11	
	(0.22)	(0.23)	(0.16)	(0.07)	(0.11)
Mn(III, 1)	0.98	0.90	0.43	0.36	
	(0.63)	(0.88)	(0.51)	(0.22)	(0.59)
Mn(III, 3)	0.68	0.58	0.32	0.29	
	(0.64)	(0.70)	(0.36)	(0.24)	(0.40)
Mn(III, 5)	0.58	0.54	0.30	0.26	
	(0.53)	(0.52)	(0.27)	(0.24)	(0.14)

[a] The values are given in parentheses.

TABLE 4: NBO Charges (in *e*) in [M(HGG)] and [M(HGGGW)(H_2O)]·$2H_2O$[a] Models

	M	N1	N2	N3	O1
Zn(II, 1)	1.58	–0.83	–0.81	–0.62	–0.68
	(1.63)	(–0.77)	(–0.80)	(–0.60)	(–0.65)
Cu(II, 2)	1.12	–0.65	–0.67	–0.54	–0.65
	(1.19)	(–0.64)	(–0.66)	(–0.53)	(–0.64)
Ni(II, 1)	0.82	–0.53	–0.57	–0.47	–0.61
	(0.83)	(–0.53)	(–0.57)	(–0.48)	(–0.64)
Ni(II, 3)	1.07	–0.61	–0.66	–0.54	–0.65
	(1.10)	(–0.61)	(–0.66)	(–0.55)	(–0.69)
Co(II, 2)	0.94	–0.59	–0.59	–0.47	–0.61
	(0.97)	(–0.53)	(–0.58)	(–0.47)	(–0.61)
Co(II, 4)	1.15	–0.65	–0.67	–0.54	–0.60
	(1.26)	(–0.65)	(–0.68)	(–0.53)	(–0.63)
Fe(II, 1)	0.80	–0.70	–0.43	–0.45	–0.65
	(0.80)	(–0.53)	(–0.58)	(–0.43)	(–0.58)
Fe(II, 3)	0.79	–0.57	–0.57	–0.48	–0.61
	(0.94)	(–0.56)	(–0.58)	(–0.47)	(–0.62)
Fe(II, 5)	1.20	–0.70	–0.69	–0.55	–0.65
	(1.31)	(–0.67)	(–0.69)	(–0.54)	(–0.64)
Mn(II, 2)	0.86	–0.60	–0.58	–0.49	–0.62
	(0.93)	(–0.57)	(–0.59)	(–0.47)	(–0.61)
Mn(II, 4)	0.95	–0.60	–0.60	–0.50	–0.62
	(1.03)	(–0.58)	(–0.60)	(–0.49)	(–0.62)
Mn(II, 6)	1.38	–0.73	–0.71	–0.57	–0.66
	(1.42)	(–0.69)	(–0.72)	(–0.55)	(–0.65)
Mn(III, 1)	0.83	–0.41	–0.45	–0.46	–0.56
	(0.84)	(–0.51)	(–0.42)	(–0.41)	(–0.58)
Mn(III, 3)	1.15	–0.49	–0.56	–0.53	–0.61
	(1.03)	(–0.51)	(–0.51)	(–0.46)	(–0.60)
Mn(III, 5)	1.32	–0.58	–0.58	–0.55	–0.64
	(1.36)	(–0.56)	(–0.57)	(–0.53)	(–0.63)

[a] The values are in parentheses.

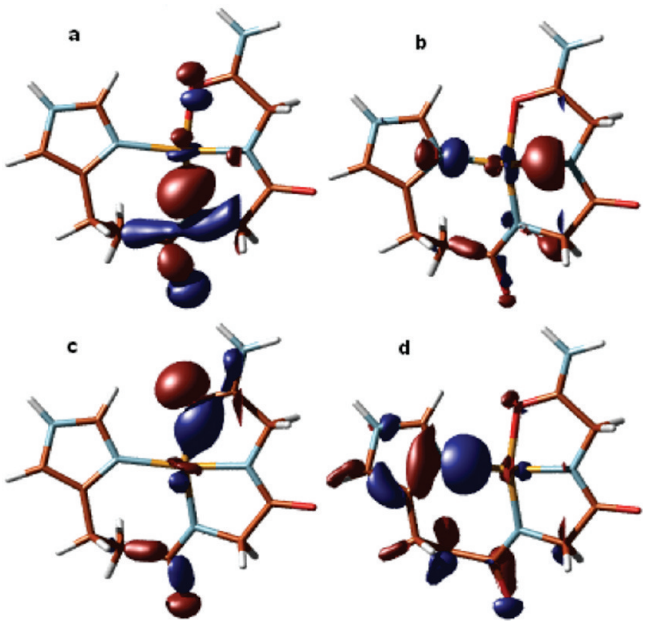

Figure 6. Schematic presentation of some relevant frontier molecular orbitals of the [Mn(HGG)].

models of PrP, HGG, and HGGGW, are negatively charged. This bonding analysis is consistent with the Mn−N1, Mn−N2, Mn−N3, and Mn−O1 bonding picture as depicted by envelope plots of selected molecular orbitals for [Mn(HGG)] (Figure 6).

M−PrP bonding energies for the studied systems have been calculated on the basis of the following scheme, in which $[M(H_2O)_4]^{n+}$ (where $n = 2$ and 3 (only for Mn(III) complexes)) was taken as a source of the transition metal cation M^{n+},

$$[M(H_2O)_4]^{n+} + [PrP]^{2-} \rightarrow [M(PrP)]^{(n-2)+} + 4H_2O \quad (2)$$

where PrP = HGG, HGGGW·3H_2O, and PrP(61−84). The calculated energies of the reactions for M = Zn(II, 1), Cu(II, 2), Ni(II, 1), Ni(II, 3), Co(II, 2), Co(II, 4), Fe(II, 1), Fe(II, 3), Fe(II, 5), Mn(II, 2), Mn(II, 4), Mn(II, 6), Mn(III, 1), Mn(III, 3), and Mn(III, 5) in the gas phase and aqueous solution (in parentheses) models are given in Table 5. One should note that we also present the gas-phase and PCM-calculated values for the model compound M[HGG], which can be compared directly with the ONIOM-calculated gas-phase data for M{PrP(61−84)} (to elucidate the effect of the proteín environment) and PCM-calculated data for the model [M(HGGGW)H_2O)]·2H_2O, respectively. In the table, we also relate the calculated M−PrP bond energies to the corresponding Cu−PrP bond energy ($\Delta\Delta E$).

As expected, Table 5 shows that reaction 1 is highly exothermic for all M cations studied. Energy changes in the gas phase are somewhat higher than those in the aqueous environment as a result of modest charge damping in the latter calculations. The gas phase ΔE values for [M{PrP(61−84)}] calculated by the ONIOM method using [M(HGG)] at a high level (DFT/BP86) are smaller than those calculated for [M(HGG)] using the DFT/BP86 level. The spin state singlet in Ni(II), doublet in Co(II), triplet in Fe(II), doublet in Mn(II), and singlet in Mn(III) are more stable than the other spin state of the respective metal. The results reveal that PrP^{2-} is a low-spin ligand. The higher stability of Mn(III) complexes is due to strong

TABLE 6: The Calculated Deformation Energy E(DEF) (kcal/mol) of the HGG^{2-} Fragment upon Coordination to the Metal Cations

M	*E*(DEF)	Δ*E*(M−Cu)
Zn(II, 1)	26.9	–3.3
Cu(II, 2)	30.2	0.0
Ni(II, 1)	42.5	12.3
Ni(II, 3)	31.9	1.7
Co(II, 2)	62.2	12.0
Co(II, 4)	30.0	–0.2
Fe(II, 1)	45.9	15.7
Fe(II, 3)	38.6	8.4
Fe(II,5)	27.8	–2.4
Mn(II, 2)	35.2	5.0
Mn(II, 4)	35.9	5.7
Mn(II, 6)	25.2	–5.0
Mn(III, 1)	51.9	21.7
Mn(III, 3)	45.6	15.4
Mn(III, 5)	44.9	14.7

TABLE 5: The Energy (kcal/mol) of the Reaction $[M(H_2O)_4]^{2+} + PrP^{2-} \rightarrow M[PrP] + 4H_2O$ Calculated at the BP86/TZVP (for PrP = HGG and [HGGGW(H_2O)]·2H_2O) and ONIOM (BP86/TZVP:Amber) (for PrP = PrP(61−84)) Levels of Theory

	PrP = HGG[d]		PrP = [HGGGW(H_2O)]·2H_2O		PrP = PrP(61−84)	
M[b]	Δ*E*[a]	Δ*E*[c]	Δ*E*	Δ*E*	Δ*E*	Δ*E*
Zn(II, 1)	–399.0 (–111.4)	19.0 (11.3)	(–171.8)	(1.9)	–296.1	8.8
Cu(II, 2)	–418.0 (–122.7)	0.0 (0.0)	(–173.7)	(0.0)	–304.9	0.0
Ni(II, 1)	–432.7 (–135.8)	–14.7 (–13.1)	(–188.0)	(–14.4)	–364.7	–59.8
Ni(II, 3)	–411.1 (–119.1)	6.9 (3.6)	(–171.2)	(2.5)	–320.8	–15.9
Co(II, 2)	–419.2 (–128.3)	–1.2 (–5.6)	(–180.4)	(–6.6)	–324.2	–19.3
Co(II, 4)	–399.0 (–108.5)	19.0 (14.2)	(–167.4)	(6.3)		
Fe(II, 1)	–379.3 (–123.9)	38.7 (–1.2)	(–143.5)	(30.2)	–272.3	32.6
Fe(II, 3)	–421.6 (–127.7)	–3.6 (–5.0)	(–176.5)	(–2.8)	–296.9	8.0
Fe(II, 5)	–395.1 (–107.4)	22.9 (15.3)	–166.7	(7.0)		
Mn(II, 2)	–408.1 (–117.4)	9.9 (5.3)	(–173.1)	(0.6)	–317.4	–12.5
Mn(II, 4)	–404.7 (–115.5)	13.3 (7.2)	(–169.3)	(4.4)		
Mn(II, 6)	–381.9 (–98.6)	36.1 (24.1)	(–161.7)	(13.0)		
Mn(III, 1)	–722.8 (–197.6)	–304.8 (–74.9)	(–273.6)	(–99.9)		
Mn(III, 3)	–703.2 (–188.6)	–285.2 (–60.9)	(–252.5)	(–78.8)		
Mn(III, 5)	–607.9 (–180.7)	–279.9 (–58.0)	(–242.3)	(–68.6)		

[a] Numbers given without and with parentheses are the gas-phase and aqueous solution phase energies, respectively. [b] The first number in the parentheses stands for the oxidation state of the metal center; the second number is the spin multiplicity of the calculated ground electronic state of the complex M[PrP]. [c] $\Delta\Delta E = \Delta E(M) - \Delta E(Cu)$. [d] In this table, we present the gas-phase and PCM-calculated values for model compound M[HGG], which can be directly compared with the ONIOM-calculated gas-phase data for M{PrP(61−84)} and PCM-calculated data for model [M(HGGGW)H_2O)]·2H_2O, respectively.

electrostatic interactions between Mn^{3+} and PrP^{2-}. The greater exothermicities of the Ni(II, 1) and Co(II, 2) ions over Cu(II, 2) is a reflection of the stronger binding to the PrP^{2-} dianion [PrP(61−84)]. The binding energies of Mn(II, 2) and Cu(II, 2) to PrP^{2-} are very similar. The results are in agreement with experimental observation that the proaggregatory effect of Mn(II) can be blocked by Cu(II).[29] The greater exothermicity in $[M(HGGGW)H_2O)]\cdot 2H_2O$ as compared to [M(HGG)] may be due in part to additional binding of one water to the M(II) in the axial position. The relative magnitude of the energy terms increases in the order Zn(II, 1) < Mn(II, 2) < Cu(II, 2) < Fe(II, 3) < Co(II, 2) < Ni(II, 1).

To investigate the substantial distortion of the prion protein upon coordination to metals, we have calculated the deformation energy (energy required to distort the model PrP from its equilibrium structure to the structure it takes in the complex; see eq 1) of model PrP in all 15 [M(HGG)] complexes. The results are compared with the copper complex in Table 6. The PrP is most distorted upon binding to Mn(III) and Fe(II) and least distorted upon binding to Zn(II). These findings correlate with the change in geometries of the systems presented in Table 1. Indeed, as seen from Table 1, angles N2−M−N3 and N1−M−O1 are distorted by ∼24.0° and 14.0° more than that in the Cu(II) system.

Conclusions

We have performed a detailed theoretical (DFT and ONIOM) study of the structure and M−PrP interaction for various M(PrP) systems (where PrP = HGG, $HGGGW\cdot 3H_2O$, and PrP(61−84)) as models of the metal-coordinated prion protein. The major findings are as follows:

1. It is predicted that Ni(II), Co(II), and Fe(II) bind more strongly to the prion protein than Cu(II), which is consistent with metal competition experiments.[44] The relative binding ability of metal ions increases in the order of Zn(II) < Mn(II, 2) < Cu(II, 2) < Fe(II, 3) < Co(II, 2) < Ni(II, 1). It was shown that (a) Cu(II) does not possess a higher affinity for PrP than dications of other first-row transition metals; (b) Mn(II) binds to the octarepeat region of the PrP; and (c) Mn(III), obtained by oxidizing Mn(II), binds more strongly to PrP than does Mn(II).

2. The geometries of the complexes for $[Mn(HGGGW)(H_2O)]\cdot 2H_2O$ are quite different for M = Mn(III) and M(II), and partial unfolding occurs only for M = Mn(III).

3. Coordination of transition metal ions to PrP(61−84) induces significant geometric changes in the PrP(61−68) and Prp(61−76) octapeptide repeat regions. The HN−NH distances between Trp(65) and Trp(73) residues are predicted to shrink by 11.26−5.68 Å. Glutamines Gln(67) and Gln(75), which participate in metal binding, also experience a reduction of H_2N-NH_2, O(CO)−O(CO), and H_2N−O(CO) distances. Both the Co(II, 2) and Mn(II, 2) complexes experience participation in a hydrogen bond between the carbonyl carbon of Gln(67) and one of the NH_2 hydrogens of Gln(75) (O···HN, 1.851 and 1.847 Å, respectively).

4. A specific aggregatory effect by Co(II) and Mn(II) is observed for [M{PrP(61−84)}]. This appears to be compatible with a previous suggestion that glutamine-cross-linked PrP may act as molecular signal stimulating endocytosis.[29] Similar effects were not observed for M = Cu(II), despite that was proposed experimentally.[44]

5. In [Zn{PrP(61−84)}], the Zn(II) dication forms a bond with the carbonyl oxygen of the Pro(84) residue in the axial position.

Acknowledgment. K.K.P. thanks the Cherry Emerson Center for Scientific Computation for a Visiting Fellowship Award. The use of computational resources at the Cherry Emerson Center for Scientific Computation is also acknowledged.

Supporting Information Available: Complete reference 42 and tables with the Cartesian coordinates of all the optimized geometries. This material is available free of charge via the Internet at http://pubs.acs.org.

References and Notes

(1) (a) Prusiner, S. B. *Proc. Natl. Acad. Sci. U.S.A.* **1998**, *95*, 13363. (b) Prusiner, S. B. *Science* **1991**, *251*, 515. (c) Prusiner, S. B. *Science* **1997**, *278*, 245. (d) Jones, C. E.; Abdelraheim, S. R.; Brown, D. R.; Viles, J. H. *J. Biol. Chem.* **2004**, *279*, 32018. (e) Knaus, K. J.; Morillas, M.; Swietnicki, W.; Malone, M.; Surewicz, W. K.; Yee, V. C. *Nat. Struct. Biol.* **2001**, *8*, 770. (f) Pushie, M. J.; Vogel, H. J. *Biophys. J.* **2007**, *93*, 3762; also see references 2−32.

(2) Weissmann, C. *Nat. Rev. Microbiol.* **2004**, *2*, 861.

(3) Prusiner, S. B. *Prion Biology and Diseases*; Cold Spring Harbor Lab. Press: Cold Spring Harbor, NY, 2003.

(4) Choi, C. J.; Kanthasamy, A.; Anantharam, V.; Kanthesamy, A. G. *NeuroToxicology* **2006**, *27*, 777, and references therein.

(5) Thompsett, A. R.; Abdelraheim, S. R.; Daniels, M.; Brown, D. R. *J. Biol. Chem.* **2005**, *280*, 42750.

(6) Millhauser, G. L. *Annu. Rev. Phys. Chem.* **2007**, *58*, 299, and references therein.

(7) Gaggelli, E.; Kozlowski, H.; Valensin, D.; Valensin, G. *Chem. Rev.* **2006**, *106*, 1995.

(8) Millhauser, G. L. *Acc. Chem. Res.* **2004**, *37*, 79, and references therein.

(9) Brown, D. R.; Wong, B. S.; Hafiz, F.; Clive, C.; Haswell, S.; Jones, I. M. *Biochem. J.* **1999**, *344*, 1.

(10) Walter, E. D.; Chattopadhyay, M.; Millhauser, G. L. *Biochemistry* **2006**, *45*, 13083.

(11) Treiber, C.; Thompsett, A. R.; Pipkorn, R.; Brown, D. R.; Multhaup, G. *J. Biol. Inorg. Chem.* **2007**, *12*, 711.

(12) Hasnain, S. S.; Murphy, L. M.; Strange, R. W.; Grossmann, J. G.; Clarke, A. R.; Jackson, G. S.; Collinge, J. *J. Mol. Biol.* **2001**, *311*, 467.

(13) Burns, C. S.; Aronoff-Spencer, E.; Legname, G.; Prusiner, S. B.; Antholine, W. E.; Gerfen, G. J.; Peisach, J.; Millhauser, G. L. *Biochemistry* **2003**, *42*, 6794.

(14) Jackson, G. S.; Murray, I.; Hosszu, L. L.; Gibbs, N.; Waltho, J. P.; Clarke, A. R.; Collinge, J. *Proc. Natl. Acad. Sci., U.S.A.* **2001**, *98*, 8531.

(15) Kramer, M. L.; Kratzin, H. D.; Schmidt, B.; Romer, A.; Windl, O.; Liemann, S.; Hornemann, S.; Kretzschmar, H. *J. Biol. Chem.* **2001**, *276*, 16711.

(16) Brown, D. R.; Guantieri, V.; Grasso, G.; Impellizzeri, G.; Pappalardo, G.; Rizzarelli, E. *J. Inorg. Biochem.* **2004**, *98*, 133.

(17) Langella, E.; Improta, R.; Barone, V. *Biophys. J.* **2004**, *87*, 3623.

(18) Colombo, M. C.; Vondele, J. V.; Doorslaer, S. V.; Laio, A.; Guidoni, L.; Rothlisberger, U. *Proteins* **2008**, *70*, 1084, and references therein.

(19) Wong, B. S.; Chen, S. G.; Colucci, M.; Xie, Z.; Pan, T.; Liu, T.; Li, R.; Gambetti, P.; Sy, M. S.; Brown, D. R. *J. Neurochem.* **2001**, *78*, 1400.

(20) Brown, D. R.; Clive, C.; Haswell, S. J. *J. Neurochem.* **2001**, *76*, 69.

(21) Brown, D. R.; Hafiz, F.; Glasssmith, L. L.; Wong, B. S.; Jones, I. M.; Haswell, S. J. *EMBO J.* **2000**, *19*, 1180.

(22) Gaggelli, E.; Bernardi, F.; Molteni, E.; Pogni, R.; Valensin, D.; Valensin, G.; Remelli, M.; Luczkowski, M.; Kozlowski, H. *J. Am. Chem. Soc.* **2005**, *127*, 996.

(23) Jones, C. E.; Klewpatinond, M.; Abdelraheim, S. R.; Brown, D. R.; Viles, J. H. *J. Mol. Biol.* **2005**, *346*, 1393.

(24) Perera, W. S.; Hooper, N. M. *Curr. Biol.* **2001**, *11*, 519.

(25) Tsenkova, R. N.; Iordinova, I. K.; Toyoda, K.; Brown, D. R. *Biochem. Biophys. Res. Commun.* **2004**, *325*, 1005.

(26) Brazier, M. W.; Davies, P.; Player, E.; Marken, F.; Viles, J. H.; Brown, D. R. *J. Biol. Chem.* **2008**, *283*, 12831.

(27) Quaglio, E.; Chiesa, R.; Harris, D. A. *J. Biol. Chem.* **2001**, *276*, 11432.

(28) Garnett, A. P.; Viles, J. H. *J. Biol. Chem.* **2003**, *278*, 6795.

(29) Giese, A.; Levin, J.; Bertsch, U.; Kretzschmar, H. *Biochem. Biophys. Res. Commun.* **2004**, *320*, 1240.

(30) Bocharova, O. V.; Breydo, L.; Salnikov, V. V.; Baskakov, I. V. *Biochemistry* **2005**, *44*, 6776.

(31) Pushie, M. J.; Rauk, A. *J. Biol. Inorg. Chem.* **2003**, *8*, 53.

(32) Riihimaki, E.-S.; Kloo, L. *Inorg. Chem.* **2006**, *45*, 8509.

(33) Parr, R. G.; Yang, W. *Density-Functional Theory of Atoms and Molecules*; Oxford University Press: New York, 1989.
(34) Koch, W.; Holthausen, M. C. *A Chemist's Guide to Density Functional Theory*, 2nd ed.; Wiley VCH: Weinheim, 2001.
(35) (a) Maseras, F.; Morokuma, K. *J. Comput. Chem.* **1995**, *16*, 1170. (b) Svensson, M.; Humbel, S.; Froese, R. D. J.; Matsubara, T.; Seiber, S.; Morokuma, K. *J. Phys. Chem.* **1996**, *100*, 19357. (c) Dapprich, S.; Komaromi, I.; Byun, K. S.; Morokuma, K.; Frisch, M. *J. Mol. Struct. THEOCHEM* **1999**, *461−462*, 1.
(36) Becke, A. D. *Phys. Rev. A* **1988**, *38*, 3098.
(37) Perdew, J. B. *Phys. Rev. B* **1986**, *33*, 8822.
(38) Schaefer, A.; Huber, C.; Ahlrichs, R. *J. Chem. Phys.* **1994**, *100*, 5829.
(39) Zahn, R. *J. Mol. Biol.* **2003**, *334*, 477.
(40) Reed, A. E.; Curtiss, L. A.; Weinhold, F. *Chem. Rev.* **1988**, *88*, 899.
(41) Babu, C. S.; Lim, C. *J. Phys. Chem. A* **2006**, *110*, 691.
(42) Frisch, M. J. *Gaussian03*; Gaussain, Inc.: Wallingford, CT, 2004.
(43) Schaftenaar, G. *MOLDEN3.4*; CAOSCAMM Center: The Netherlands, 1998.
(44) Burns, C. S.; Aronoff-Spencer, E.; Dunham, C. M.; Lario, P.; Avdievich, N. I.; Antholine, W. E.; Olmstead, M. M.; Vrielink, A.; Gerfen, G. J.; Peisach, J.; Scott, W. G.; Millhauser, G. L. *Biochemistry* **2002**, *41*, 3991.
(45) Webb, S. M.; Dick, G. J.; Bargar, J. R.; Tebo, M. *Proc. Natl. Acad. Sci.* **2005**, *102*, 5558.
(46) Hansel, C. M.; Francis, C. A. *Appl. Environ. Microbiol.* **2006**, *72*, 3543.
(47) Wiberg, K. A. *Tetrahedron* **1968**, *24*, 1083.

JP909945E